한국소음진동공학회 1997년도 춘계학술대회논문집, pp. 701 ~ 708.

# 일반 경계 조건을 가진 얇은 물체에 대한 직접 경계 요소법의 개발

0이 강 덕*, 이 덕 주**

# Development of the direct boundary element method for thin bodies with general boundary conditions

Kang-Duck Ih, Duck-Joo Lee

## ABSTRACT

A direct boundary element method (DBEM) is developed for thin bodies whose surfaces are rigid or compliant. The Helmholtz integral equation and its normal derivative integral equation are adopted simultaneously to calculate the pressure on both sides of the thin body, instead of the jump values across it, to account for the different surface conditions of each side. Unlike the usual assumption, the normal velocity is assumed to be discontinuous across the thin body. In this approach, only the neutral surface of the thin body has to be discretized. The method is validated by comparison with analytic and/or numerical results for acoustic scattering and radiation from several surface conditions of the thin body; the surfaces are rigid when stationary or vibrating, and part of the interior surface is lined with a sound-absorbing material.

## 1. Introduction

Studies show that the conventional boundary element method (BEM) using the Helmholtz integral equation fails to yield reliable results for thin bodies. The major reason for this failure comes from the nearly singular integral owing to the mesh on one side of the thin body being too close to the mesh on the opposite side.

Seybert *et al.* [1] adopted a multi-domain BEM formulation for the thin-body acoustic problem in which a fictitious interface surface is constructed to divide the acoustic field into several subdomains. As a result, the Helmholtz integral equation for a fictitious thick body enclosed by the thin body surface and the fictitious surface is to be solved in a straightforward manner. Even though the concept of the multi-domain BEM is simple, it requires great effort in preprocessing to construct the mesh and also results in a very large system of equations if the fictitious surface is relatively large.

Martinez [2] defined the failure as a thin-shape breakdown (TSB) and showed that a normal derivative of the Helmholtz integral equation approach provides a robust formulation for the thin body with a systematic analysis for a rigid wall or a state of continuous normal motion of flapping. However, the normal derivative integral equation has the hypersingular integral in the order of $O(1/r^3)$ so that the special technique to

* 현대자동차(주) 차량시험 2 팀
** 한국과학기술원 항공우주공학과 정회원

regularize the hypersingular integral is necessary.

In a direct boundary element method (DBEM) approach, Wu & Wan [3] proved that the same failure problem cannot be fixed by DBEM because the Helmholtz integral equation becomes degerate. They solved the normal derivative integral equation formulation for the thin body with a less singular normal derivative integral equation, derived by Maue [4] and later by Mitzner [5]. Detailed discussions about the regularization of the hypersingular integral is summarized in [6]. Recently, the method was applied to a regular body with thin fins and a vibrating surface on the regular body by solving a mixed thin-body and regular-body integral formulation [7].

In addition to the above mentioned works, different approaches have been carried out for the thin-body problem. Hamdi and Ville [8] and Wu *et al.* [9] used a variational formulation. Malbéqui *et al.* [10] used an indirect boundary element method (IDBEM) to a duct, which was assumed to be hard-walled both inside and outside. Martinez, using a modal boundary integral technique, analyzed the acoustic diffraction due to a sound source by the open-ended cylindrical duct. Here the interior surface of the duct was rigid [11] and/or with a compliant lining [12]. Treatment of the thin-body problem with a compliant lining by using DBEM for the normal derivative integral equation formulation was not reported.

In this paper, a new DBEM is reformulated to extend to thin bodies with rigid and compliant surface using the combined Helmholtz integral equation and the combined normal derivative integral equation. This can be done by removing the normal velocity continuation assumption across the thin body. The hypersingular integral is regularized by using the Maue's less singular normal derivative integral equation. The numerical integration is carried out using a standard Gaussian quadrature. The collocation points are at the nodal points for the combined Helmholtz integral equation and inside each element for the combined normal derivative integral equation to confirm the condition at the corner and the vertex. The knife-edge effect is treated by adopting a quarter-point element [14-16].

## 2. Integral formulation for the thin body coated in different materials

Fig. 1 depicts the mathematical notations for a thin body coated in different materials on each side in the homogeneous acoustic medium. The acoustic field is temporally divided into two parts (the exterior subdomain $\Omega^+$ and the interior subdomain $\Omega^-$) by an imaginary surface, $s$, to formulate a new integral equation for the thin body [1, 3]. The thin body is mathematically discribed by a neutral surface, $S$, because the surface exposed to each subdomain is assumed to be coated in different materials. The velocity potential in the subdomain $\Omega^-$ is denoted by $\phi^-$, the velocity potential in $\Omega^+$ is $\phi^+$ and the acoustic source is $\phi_s$. The velocity potential is defined as $\vec{v} = -\nabla\phi$ and the $e^{+i\omega t}$ convention for time harmonic analysis is used. Then, the acoustic pressure can be calculated by $p = ik\rho_0 a_0 \phi$, where $i = \sqrt{-1}$, $k = \omega / a_0$ is the wave number, $\rho_0$ is the density of acoustic medium and $a_0$ is the speed of sound.

By applying Green's theorem to the Helmholz equation, the Helmholtz integral equation for each subdomain is obtained as shown below:

$$C^+(P)\phi^+(P) = -\int_{S+s} G(P,Q)\frac{\partial\phi^+(Q)}{\partial n} - \frac{\partial G(P,Q)}{\partial n}\phi^+(Q)dS(Q) \quad (1)$$

and

$$C^-(P)\phi^-(P) = \int_{S+s} G(P,Q)\frac{\partial\phi^-(Q)}{\partial n} - \frac{\partial G(P,Q)}{\partial n}\phi^-(Q)dS(Q) + 4\pi\phi_*(P,X_*) \quad (2)$$

where $P$ is the collocation point, $Q$ is the secondary source point on the surface and $X_*$ is the acoustic source point. The surface integral is applied to $S+s$. The symbols $C^-, C^+$ represent the solid angles at $P$ in the exterior and interior subdomains respectively. The kernel function $G(P,Q)$ is the free space Green's function, $G(P,Q) = e^{-ikr}/r$, in which $r = |Q-P|$.

Adding equation (1) and equation (2) results in a single equation (the combined Helmholtz integral equation):

$$\begin{aligned} &C^+(P)\phi^+(P) + C^-(P)\phi^-(P) \\ &= -\int_S G(P,Q)\left(\frac{\partial\phi^+(Q)}{\partial n} - \frac{\partial\phi^-(Q)}{\partial n}\right)dS(Q) \\ &+ \int_S \frac{\partial G(P,Q)}{\partial n}\left(\phi^+(Q) - \phi^-(Q)\right)dS(Q) \\ &+ 4\pi\phi_*(P,X_*) \end{aligned} \quad (3)$$

The first part of right hand side, usually canceled for the rigid surface because of the continuous normal velocity, is included in the above equation. The integrations on the imaginary surface are canceled because of the continuity of pressure and particle velocity on that fictitious surface.

By taking the normal derivative to equation (3), another combined normal derivative integral equation is obtained:

$$\begin{aligned} &C^+(P)\frac{\partial\phi^+(P)}{\partial n_p} + C^-(P)\frac{\partial\phi^-(P)}{\partial n_p} \\ &= -\int_S \frac{\partial G(P,Q)}{\partial n_p}\left(\frac{\partial\phi^+(Q)}{\partial n} - \frac{\partial\phi^-(Q)}{\partial n}\right)dS(Q) \\ &+ \int_S \frac{\partial^2 G(P,Q)}{\partial n_p \partial n}\left(\phi^+(Q) - \phi^-(Q)\right)dS(Q) \\ &+ 4\pi\frac{\partial\phi_*(P,X_*)}{\partial n_p} \end{aligned} \quad (4)$$

The general boundary conditions on both sides are given by:

$$\frac{\partial\phi^+}{\partial n} = -\alpha^+\phi^+ - \beta^+, \quad \frac{\partial\phi^-}{\partial n} = \alpha^-\phi^- + \beta^- \quad (5a, 5b)$$

where $\alpha^\pm = i\rho_0 a_0 k Y^\pm$ are coefficients related to the acoustic admittance($Y^\pm$) and $\beta^\pm$ are normal vibration velocities on each side of the thin body surface.

Special conditions to treat the diffraction effect at the knife edge are:

$$\phi^+ = \phi^- \quad (5c)$$

After applying the boundary conditions, equations (5a) and (5b), to equations (3) and (4), two integral equations with two unknowns $\phi^+$ and $\phi^-$ on the surface can be deduced as:

$$\begin{aligned} &C^+\phi^+(P) + C^-\phi^-(P) \\ &= \int_S\left(\alpha^+ G(P,Q) + \frac{\partial G(P,Q)}{\partial n}\right)\phi^+(Q)dS(Q) \\ &+ \int_S\left(\alpha^- G(P,Q) - \frac{\partial G(P,Q)}{\partial n}\right)\phi^-(Q)dS(Q) \\ &+ \int_S\left(\beta^+ + \beta^-\right)G(P,Q)dS(Q) + 4\pi\phi_*(P,X_*) \end{aligned} \quad (6)$$

and

$$\begin{aligned} &2\pi\alpha^+\phi^+(P) - 2\pi\alpha^-\phi^-(P) \\ &= \int_S\left(\alpha^+\frac{\partial G(P,Q)}{\partial n_p} + \frac{\partial^2 G(P,Q)}{\partial n_p \partial n}\right)\phi^+(Q)dS(Q) \\ &+ \int_S\left(\alpha^-\frac{\partial G(P,Q)}{\partial n_p} - \frac{\partial^2 G(P,Q)}{\partial n_p \partial n}\right)\phi^-(Q)dS(Q) \\ &+ \int_S\left(\beta^+ + \beta^-\right)\frac{\partial G(P,Q)}{\partial n_p}dS(Q) \\ &+ 4\pi\frac{\partial\phi_*(P,X_*)}{\partial n_p} + 2\pi\left(\beta^+ - \beta^-\right) \end{aligned} \quad (7)$$

## 3. Treatment of problems in the integral equation

It is well known that the integration has some problems: the integration of the singular kernel, the treatment of singularity near the knife edge, the non-uniqueness of the solution, and the treatment of the corner and the vertex. The following approaches were

adopted to solve these integration problems.

First, the kernel $\partial^2 G / \partial n_p \partial n$ is hypersingular in the order of $O(1/r^3)$; therefore, an acceptable result cannot be obtained in this case. So, it is essential to reduce the order of singularity. Putting collocation points inside each element satisfies the $C^1$ continuity condition and makes it possible to use the following important relation derived by Maue [4] and later by Mizner [5]:

$$\int_S \frac{\partial^2 G}{\partial n_p \partial n}\phi dS = \int_S [(\hat{n}_p \times \nabla_p G)\cdot(\hat{n}\times\nabla\phi) + k^2(\hat{n}_p\cdot\hat{n})G\phi]dS \quad (8)$$

The order of singularity then becomes $O(1/r^2)$. And adopting the local polar coordinates reduces the order of singularity to $O(1/r)$ again. Now, the standard Gaussian quadrature can be applied to the reduced integrations. In this paper, the singular integration is carried out using the method in [13], based on the Cauchy principal integration.

Second, the acoustic velocity potential has a singularity at the knife edge in the order of $O(1/\sqrt{r})$. Even using a fine mesh of higher-order elements will not produce sufficient accuracy. By using node-shift elements or quarter-point elements, the knife edge singularity can be overcome easily [3, 15, 16].

Third, the non-uniqueness problem (occurring at some frequencies related to the eigen values of the corresponding interior region of the body) is not severe in the thin body case. Because the number of eigen values for a particular geometry is given approximately as:

$$n_{eigen} = \frac{Vk^3}{6\pi^2} \quad (9)$$

where $V$ is the volume of the body. For a thin body, $V$ is zero. Therefore, it is not necessary to consider the non-uniqueness problem in this case [7].

The final problem is how to treat the solid angle effect at the corner or the vertex. The collocation points that are placed inside the elements cannot represent the solid angles at the corners or vertexes. We used two kinds of collocation points on each element. For equation (6), collocation points are placed on the boundary of the element to calculate the correct solid angle. For equation (7), collocation points are placed inside the elements to use the equation (8). The configurations of the master elements for equations (6) and (7) are shown in Fig. 2.

## 4. Numerical implementation

An isoparametric eight-node quadrilateral and six-node triangular element is used in this paper. *i.e.*,

$$x_i(\vec{\xi}) = \sum_\alpha N_\alpha(\vec{\xi}) X_{i\alpha} \quad (i = 1,2,3);$$
$$\phi(\vec{\xi}) = \sum_\alpha N_\alpha(\vec{\xi})\Phi_\alpha (\alpha = 1,2,\cdots,6 \text{ or } 8) \quad (10)$$

A system equation can be deduced from equations (6) and (7):

$$\begin{bmatrix} A_{++} & A_{+-} \\ A_{-+} & A_{--} \end{bmatrix} \begin{Bmatrix} \Phi^+ \\ \Phi^- \end{Bmatrix} = \begin{Bmatrix} F_+ \\ F_- \end{Bmatrix}. \quad (11)$$

Components in the matrix are defined as appendix A:

## 5. Results and discussions

To verify our present method, firstly, the scattering problem of a plane wave from a rigid circular disk of radius, $a$, is tested. The incident velocity potential is given as $\phi_{sc} = e^{-ikx}$. For the comparison of our results with [3], the same mesh is used: 16 eight-node quadrilateral elements and 32 six-node triangular elements, as shown in Fig. 3. Calculated non-dimensional wavenumbers, $ka$, are 1, 2, 3, 4 and 5. For the rigid body, the admittances on both surfaces, $\alpha^+, \alpha^-$, are zero and $\beta^+, \beta^-$ are also set to zero. Fig.s 4 shows the real and the imaginary parts of the relative scattered velocity potential on the illuminated side. By comparison with the analytic solution, both results in [3]

and the present calculations show excellent agreements.

The second case tested the radiation by a vibrating circular disk. The radiation problem has the exactly same solution of the scattered field. However, the boundary conditions to calculate for each case are different. For the scattering problem, $\alpha^+, \alpha^-$, $\beta^+, \beta^-$ are zero; and for the radiation case, $\alpha^+, \alpha^-$ are also zero but $\beta^+, \beta^-$ are set equal to the surface-vibrating velocity. The test results are depicted in the Fig. 5. Good agreement with the analytic solution is also observed.

The next problem is the scattering of an incident plane wave from a rigid thin-walled cylinder open at one end. The radius of the open cylinder is $a$ and the length is $2a$. The mesh used to model this open cylindrical shell consists of 40 eight-node quadrilateral elements and eight six-node triangular elements, as shown in Fig. 6. Quarter points (flooded circle) rather than middle points (hollow circle), are used for the elements adjacent to the knife edge, which is at the open end of the cylinder. The incident plane wave has a velocity potential of unit amplitude and is assumed to impinge on the cylinder from the open end. The effect of locations of collocation points is shown in Fig. 7. Herein, only the mesh (b) in Fig. 2 is used for the present calculation and the result is compared with that of Wu and Wan [3]. This result indicates that the mesh (a) in Fig. 2 should be used for the combined Helmholtz integral equation and the mesh (b) for the combined normal derivative integral equation. Fig. 8 gives the comparison between the present BEM, using meshes (a) and (b) in Fig. 2 for equations (6) and (7) respectively, and the Wu and Wan's solution for the scattered potentials on both sides (exterior and interior) of the cylindrical surface. The real and imaginary parts of the scattered velocity potentials on the side wall as a function of $z$ are showed in Fig.s 8(a) and (b) respectively. Fig. 8(c) shows the real parts of the scattered velocity potentials on the bottom wall as a function of $r$, and Fig. 8(d) shows the corresponding imaginary parts. Again, a good agreement is observed. These results indicate that the treatment of the solid angle by the present method is reasonable at the corner or vertex.

Finally, the present BEM is applied to a thin body having general boundary conditions. The scattering of an incident plane wave from a cylindrical shell open at one end is shown in Fig. 9. The inside bottom surface is assumed to be partly coated with an absorbing material. The radius of the coated area is $a/2$ and the coefficient is taken as $\alpha^- = k^2 3^{-1}(1+i0.3)^{-1}$. The results from the present method is compared with those obtained by the multi-domain method [1]. The scattered velocity potentials on the surface are depicted in Fig. 10. From the data in Fig.s 10, it is shown that the results obtained by the present BEM and the multi-domain BEM agree well for the cases that have different boundary conditions across the thin body.

## 6. Conclusion

A direct boundary element method (DBEM) is reformulated to extend to thin bodies with rigid and compliant surfaces by removing the normal velocity continuation assumption. The combined Helmholtz integral equation and the combined normal derivative integral equation are solved simultaneously to account for the different boundary conditions on the surfaces across the thin body. The different locations of the collocation point in the two integral equations is critical to take account of the reasonable solid angle effect. The knife edge effect is considered to confirm the knife-edge condition by using a quarter-point element. No fictitious surfaces are required in this formulation. Therefore, the discretization is only restricted on the neutral surface of the thin bodies. The present method can be easily

applied to the problem of scattering and radiation from thin bodies of arbitrary shape having either rigid and compliant surfaces.

## 7. References


1. A.F.Seybert, C.Y.R.Cheng and T.W.Wu 1990 *Journal of the Acoustical Society of America* **88**, 1612-1618. The solution of coupled interior/exterior acoustic problems using the boundary element method.
2. R.Martinez 1991 *Journal of the Acoustical Society of America* **90**, 2728-2738. The thin-shape breakdown(TSB) of the Helmholtz integral equation.
3. T.W.Wu and G.C.Wan 1992 *Journal of the Acoustical Society of America* **92**, 2900-2906. Numerical modeling of acoustic radiation and scattering from thin bodies using a Cauchy principal integral equation.
4. A.W.Maue 1949 *Zeischrift der Physik* **126**, 601-618. Zur formulierung eines allegemeinen beugungsproblems durch eine integralgleichung.
5. K.M.Mitzner 1966 *Journal of Mathematical Physics* 7, 2053-2060. Acoustic scattering from an interface between media of greatly different density.
6. M.Tanaka, V.Sladek and S.Sladek 1994 *Applied Mechanics Reviews* **47**, 457-499. Regularization techniques applied to boundary element method.
7. T.W.Wu 1995 *Journal of the Acoustical Society of America Journal* **97**, 84-91. A direct boundary element method for acoustic radiation and scattering from mixed regular and thin bodies.
8. M.A.Hamdi and J.M.Ville 1986 *Journal of Sound and Vibration* **107**, 231-242. Sound radiation from ducts: theory and experiment.
9. X.F.Wu, A.D.Pierce and J.H.Ginsberg 1987 *IEEE Journal of Osceanic Engineering* **OE-12**, 412-418. Variational method for computing surface acoustic pressure on vibrating bodies, applied to transversely oscilliating disks.
10. P.Malbéqui, C.Glandier and C.Reynier 1993 *AIAA Aeroacoustic Conference at Long Beach, CA* **93-4376**. Anaysis of sound propagation and radiation in a curved duct using a boundary integral method: comparison with experiment.
11. R.Martinez 1988 *American Institute of Aeronautics and Astronautics Journal* **26**, 396-404. Diffracting open-ended pipe treated as a lifting surface.
12. R.Martinez 1990 *Journal of the Acoustical Society of America* **87**, 523-531. A boundary integral formulation for thin-walled shapes of revolution.
13. T.W.Wu, A.F.Seybert and G.C.Wan 1991 *Journal of the Acoustical Society of America* **90**, 554-560. On the numerical implementation of Cauchy principal value integral to insure a unique solution for acoustic radiation and scattering.
14. A.F.Seybert, Z.H.Jia and T.W.Wu 1992 *Journal of the Acoustical Society of America* **91**, 1278-1283. Solving knife-edge scattering problems using singular boundary elements.
15. D.Henshell 1975 *International Journal for Numerical Methods in Engineering* **9**, 495-507. Crack tip finite elements are unnecessary.
16. R.Barsoum 1976 *International Journal for Numerical Methods in Engineering* **10**, 25-37. On the use of isoparametric finite elements in linear fracture mechanics.


## Appendix A

$$A_{++} = -\int_{S_m}\left[\alpha^{+}(Q(\vec{\xi}))G(P,Q(\vec{\xi})) + \frac{\partial G(P,Q(\vec{\xi}))}{\partial n}\right]N(\vec{\xi})dS_m \qquad (12a)$$

$$A_{+-} = -\int_{S_m}\left[\alpha^{-}(Q(\vec{\xi}))G(P,Q(\vec{\xi})) - \frac{\partial G(P,Q(\vec{\xi}))}{\partial n}\right]N(\vec{\xi})dS_m \tag{12b}$$

$$A_{-+} = -\int_{S_m}\left[\alpha^{+}(Q(\vec{\xi}))\frac{\partial G(P,Q(\vec{\xi}))}{\partial n_p} + \frac{\partial^2 G(P,Q(\vec{\xi}))}{\partial n \partial n_p}\right]N(\vec{\xi})dS_m \tag{12c}$$

$$A_{--} = -\int_{S_m}\left[\alpha^{-}(Q(\vec{\xi}))\frac{\partial G(P,Q(\vec{\xi}))}{\partial n_p} - \frac{\partial^2 G(P,Q(\vec{\xi}))}{\partial n \partial n_p}\right]N(\vec{\xi})dS_m \tag{12d}$$

$$F_{+} = \int_S(\beta^{+}+\beta^{-})G(P,Q(\vec{\xi}))dS + 4\pi\phi_{sc}(P,X_{sc}) \tag{12e}$$

$$F_{-} = \int_S(\beta^{+}+\beta^{-})\frac{\partial G(P,Q(\vec{\xi}))}{\partial n_p}dS + 4\pi\frac{\partial \phi_{sc}(P,X_{sc})}{\partial n_p} + 2\pi\{\beta^{+}-\beta^{-}\} \tag{12f}$$

where $N(\vec{\xi}) = \{N_1, N_2, \cdots, N_6 \text{ or } N_8\}$ and $\Phi^{\pm}$ is the column vectors of the velocity potential

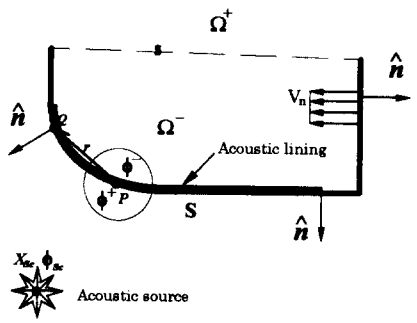


Fig. 1. Mathematical model for a thin-body coated in different materials.

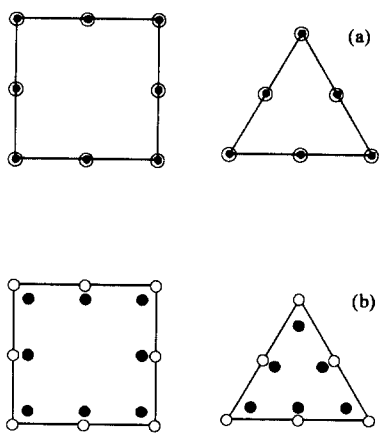


Fig. 2. Configuration of the master elements. (a) master elements for equation (6); (b) master elements for equation (7). (hollow circle : nodal points; flooded circle : collocation points)

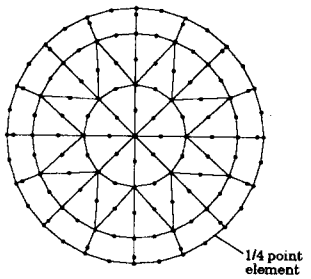


Fig. 3. Mesh for a disk problem.

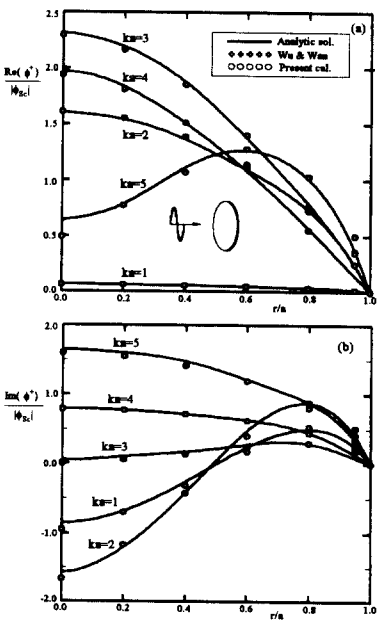


Fig. 4. Normalized scattered velocity potential on the illuminated surface.

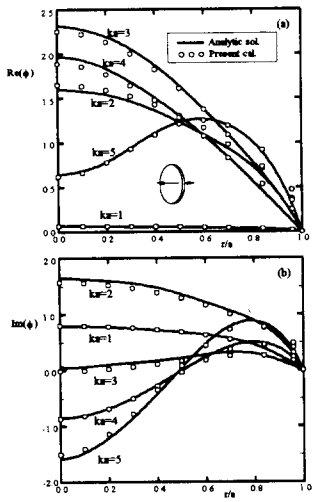


Fig. 5. Normalized velocity potential of the vibrating circular disk.

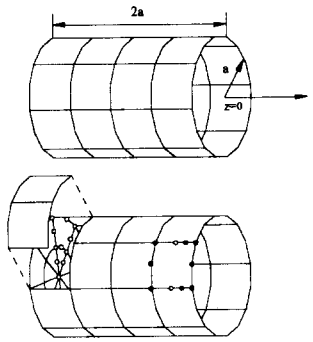


Fig. 6. Duct geometry and the used mesh. 40 eight-node quadrilateral and 8 six-node triangular elements are used. (Flooded circle: element for the knife edge, hollow circle: regular element)

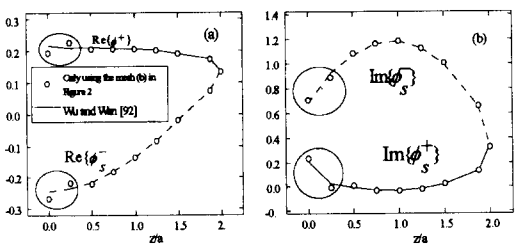


Fig. 7. Solid-angle effect at corners and vertexes. Solid and dotted lines represent the results of Wu and Wan's calculation in [3]. Hollow circle is the result by using $C^1$ element for both equations (6) and (7). Plotted quantity is the scatterd velocity potential on the surface of the wall. (a) Real part on the side wall; (b) Imaginary part on the side wall

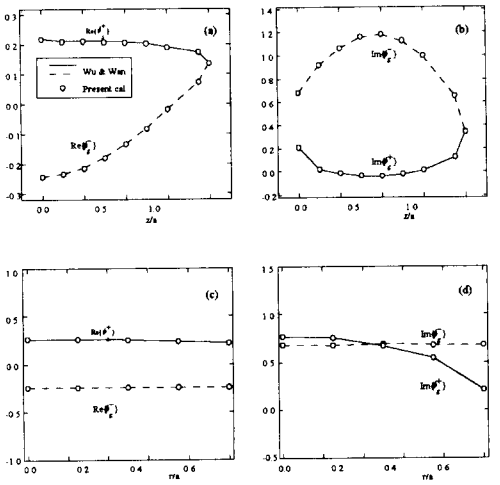


Fig. 8. Scattered velocity potential on the wall surface. (a) Real parts on the side wall; (b) Imaginary parts on the side wall;(c) Real parts on the bottom wall; (d) Imaginary parts on the bottom wall.

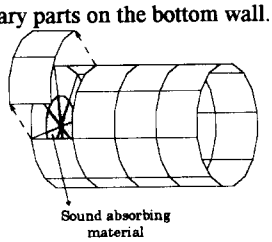


Fig. 9. Circular cylindrical shell in which a sound absorbing material is partly mounted.

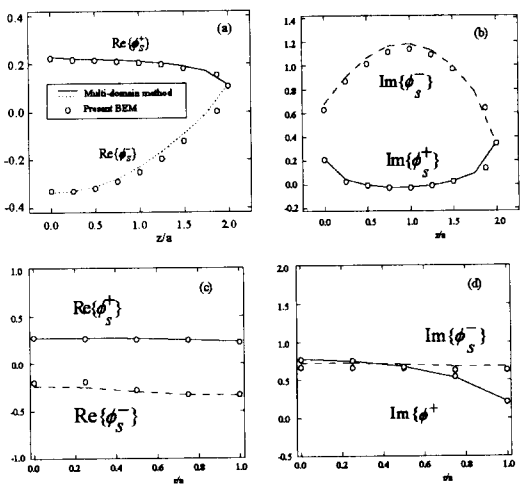


Fig. 10. Scattered velocity potential on the wall surface when $ka$=1.0 and the absorbing material with $\alpha = k^2 3^{-1}(1+i0.3)^{-1}$ is partly covered on the inner side of bottom surface. ( $r = \sqrt{x^2 + y^2}$ )